Submitted to the 29th International Conference on High-Energy Physics ICHEP98,
Vancouver, Canada, July 1998

Diffractive Dijet Production at HERA

H1 Collaboration

Abstract

Interactions of the type $ep \to eXY$ are studied, where the component X of the hadronic final state contains two jets and is well separated in rapidity from a leading baryonic system Y. Analyses are performed of both resolved and direct photoproduction and of deep-inelastic scattering with photon virtualities in the range $7.5 < Q^2 < 80\ \mathrm{GeV}^2$. Cross sections are presented where Y has mass $M_Y < 1.6$ GeV, the squared four-momentum transferred at the proton vertex satisfies $|t| < 1\ \mathrm{GeV}^2$ and the two jets each have transverse momentum $p_T^{\mathrm{jet}} > 5$ GeV relative to the photon direction in the rest frame of X. Models based on a factorisable diffractive exchange with a gluon dominated structure, evolved to a scale set by the transverse momentum $\hat{p}_T$ of the outgoing partons from the hard interaction, give good descriptions of the data. Exclusive $q\bar{q}$ production, as calculated in perturbative QCD using the squared proton gluon density, represents at most a small fraction of the measured cross section. The compatibility of the data with a breaking of diffractive factorisation due to spectator interactions in resolved photoproduction is investigated.

Abstract: 566
Parallel sessions: 5,3
Plenary sessions: 7,5

1 Introduction

The concept of a pomeron ($\mathbb{P}$) trajectory possessing vacuum quantum numbers and mediating diffractive scattering has proved remarkably successful in formulating a Regge description of high energy hadronic cross sections[1]. There has been considerable recent interest in understanding the underlying dynamics of diffractive interactions in terms of quantum chromodynamics (QCD). If the pomeron can be considered as a partonic system[2], then perturbatively calculable processes involving large transverse momenta are expected. High transverse momentum jet production has been observed in diffractive $p\bar{p}$ scattering [3, 4, 5] and also in photoproduction at HERA[6, 7, 8].

At HERA, diffractive scattering is studied both in photoproduction and at large Q^2 using events of the type $ep \to eXY$, where the hadronic systems X and Y are separated by a large region of pseudorapidity that is devoid of hadronic activity [9, 10] and Y is predominantly a proton [11]. The contribution from such processes to the total photoproduction cross section at γp centre of mass energies $W \sim 200$ GeV exceeds 20% [12, 13]. The leading twist large rapidity gap component represents approximately 10% of the total deep-inelastic scattering (DIS) cross section [14, 15, 16].

The contribution to the proton structure function from the process $ep \to eXY$ ($M_Y < 1.6$ GeV, $|t| < 1$ GeV^2) has been measured differentially in the fraction $x_{\mathbb{P}}$ of the proton beam momentum transferred to the system X. The results [16] have been presented in terms of a structure function $F_2^{D(3)}(x_{\mathbb{P}}, \beta, Q^2)$ where $\beta = x/x_{\mathbb{P}}$ and x is the Bjorken scaling variable. A Regge analysis of $F_2^{D(3)}$ demonstrates that diffraction is dominant at small $x_{\mathbb{P}}$, with sub-leading exchanges ($\mathbb{R}$) becoming important as $x_{\mathbb{P}}$ increases. The β and Q^2 dependence of $F_2^{D(3)}$ has been considered in terms of the QCD evolution of a structure function for the pomeron [14, 16]. Assuming that the evolution for $\beta < 0.65$ is governed by the DGLAP[17] equations, diffractive parton distributions are extracted that are dominated at low Q^2 by gluons carrying large fractions of the exchanged momentum (referred to as `hard' gluons in this paper). Under the hypothesis of diffractive factorisation, the parton distributions for the pomeron extracted from $F_2^{D(3)}$ are expected to describe diffractive interactions wherever perturbation theory may be applied.

Complementary to the approach based on pomeron parton distributions, diffractive $\gamma^* p$ interactions have also been modelled in terms of the elastic scattering from the proton of partonic fluctuations of the photon, which at high energy develop well in advance of the target. The kinematic dependences expected for the distinct photon fluctuations are very different. For the simplest $q\bar{q}$ state, the colour transparency mechanism suppresses the cross section when the transverse separation of the two partons is small [18]. The $q\bar{q}$ cross section is therefore expected to be significant only at comparatively small transverse momenta $\hat{p}_T$ of the outgoing partons in the centre of mass frame of the hard interaction. In this case, the entire diffractive mass M_X is shared by the $q\bar{q}$ pair. Several calculations [19, 20, 21] have been performed, the scattering of the $q\bar{q}$ pair from the proton being modelled by the exchange of two gluons in a net colour singlet configuration [22]. In contrast to the $q\bar{q}$ state, the colour transparency effect is prevented for photon fluctuations with additional low transverse momentum gluons. At large $\hat{p}_T$ the cross section is therefore expected to be dominated by the scattering of $q\bar{q}g$ and higher multiplicity components of the photon. This conclusion is reached both in two gluon exchange models [20] and in a semi-classical model [23] in which the partonic photon fluctuations are scattered in the proton colour field [24]. A recent parameterisation in terms of contributions from $q\bar{q}$ and $q\bar{q}g$ states can give an acceptable description of $F_2^{D(3)}$ data [25].

Several hadronic final state observables are sensitive to the partonic structure of diffractive interactions. The parton distributions extracted from the QCD analysis of $F_2^{D(3)}$ are able to describe measurements of event thrust[26], energy flow, charged particle spectra[27] and charged particle multiplicities and their correlations[28] in diffractive DIS. Viewed in terms of photon fluctuations, these measurements confirm the need for Fock states with one or more gluons at comparatively large M_X and high $\hat{p}_T$.

In this paper, large rapidity gap events that contain two high transverse momentum jets as components of the system X are investigated in separate analyses of photoproduction and DIS data. Cross section measurements are presented differentially in the jet pseudorapidity in the laboratory frame, in the jet momentum transverse to the $\gamma^{(*)}$ axis in the rest frame of the system X and in the fractions of the photon and pomeron momenta that are transferred to the dijet system. The data are compared to predictions based on diffractive parton densities extracted from $F_2^{D(3)}$ at a scale set by $\hat{p}_T$. In diffractive interactions where both colliding particles can interact strongly, it has been argued that the factorisation property for diffractive parton distributions is at best approximate, since additional soft interactions among spectator partons may couple the extended hadrons to one another [29, 30, 31]. The possible presence of such an effect in resolved photoproduction, where the photon interacts through its hadronic structure, is investigated. A model of the contribution to the diffractive DIS cross section from the $q\bar{q}$ fluctuation of the photon [21] is also compared to the data. A further comparison is made with an inclusive model of DIS in which soft interactions produce rapidity gaps by altering the colour connections between outgoing partons [32].

In section 2, kinematic variables are introduced and the measured processes are defined at the level of final state hadrons. Section 3 introduces the Monte Carlo models which are used to determine corrections to the data. The components of the H1 detector most relevant to the analysis, the event selection and reconstruction methods are covered in section 4, along with further details of the experimental procedure. The measured cross sections are presented and discussed in section 5.

2 Kinematic variable and cross section definitions

The hadronic final state is considered here in terms of the generic quasi-two body photon-proton interaction $\gamma^{(*)}p \rightarrow XY$, as illustrated in figure 1a. By definition, the systems X and Y are separated by the largest gap in the rapidity distribution of final state hadrons and Y is the system closest to the outgoing proton direction [12, 16].

With k and P denoting the 4-vectors of the incoming electron and proton respectively and q the 4-vector of the photon, the standard kinematic variables

$$s \equiv (k+P)^2 \qquad Q^2 \equiv -q^2 \qquad W^2 \equiv (q+P)^2 \qquad y \equiv \frac{q \cdot P}{k \cdot P} \tag{1}$$

are defined. With p_X and p_Y representing the 4-vectors of the two distinct components of the hadronic final state in the context of figure 1a, the data are also discussed in terms of

$$M_X^2 \equiv p_X^2 \qquad M_Y^2 \equiv p_Y^2 \qquad t \equiv (P - p_Y)^2 \qquad x_{\mathbb{P}} \equiv \frac{q \cdot (P - p_Y)}{q \cdot P}\,, \tag{2}$$

where M_X and M_Y are the invariant masses of X and Y, t is the squared four-momentum transferred between the photon and the incoming proton and $x_{\mathbb{P}}$ is the fraction of the proton

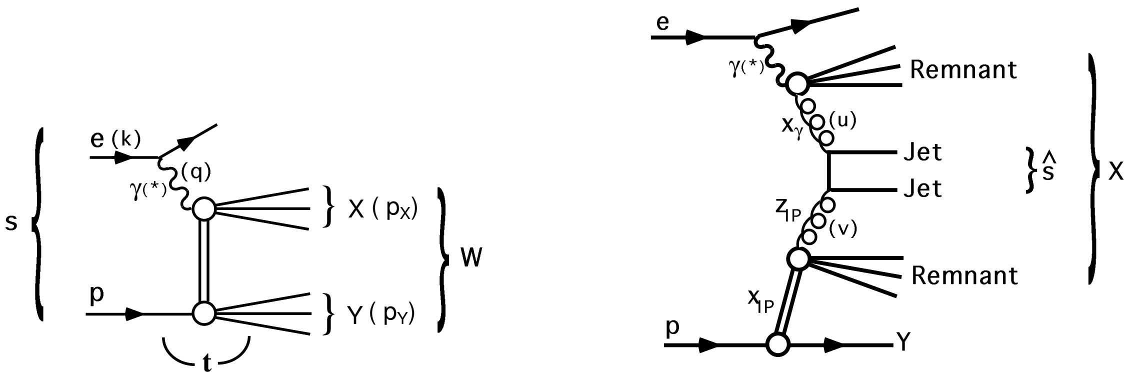

(a) **(b)**

Figure 1: (a) Illustration of the generic process, $ep \to eXY$, in which the largest gap in the rapidity distribution of final state hadrons separates the systems X and Y, associated with the photon and proton vertices respectively. (b) An example diffractive dijet production process in which the photon is resolved. The partons entering the hard interaction from the photon and the pomeron have 4-momenta u and v and carry momentum fractions x_γ and $z_{\mathbb{P}}$ respectively.

beam momentum transferred to the system X. Further kinematic variables are defined for use in the large Q^2 regime:

$$x \equiv \frac{Q^2}{2q \cdot P} \qquad\qquad \beta \equiv \frac{x}{x_{\mathbb{P}}} \equiv \frac{Q^2}{2q \cdot (P - p_Y)} \ , \tag{3}$$

where β may be interpreted in the proton infinite momentum frame as the fraction of the exchanged 4-momentum that is carried by the quark coupling to the photon.

Further variables describing the hard interaction are introduced for the case of dijet production. Assuming a "$2 \to 2$ parton" interaction of the kind shown in figure 1b, the system X generally contains low transverse momentum remnants of the photon and of the pomeron. If the partons from the photon and the pomeron entering the hard scattering have 4-momenta u and v respectively, the dijet system has squared invariant mass

$$\hat{s} \equiv (u + v)^2 \ , \tag{4}$$

and the projections

$$x_\gamma \equiv \frac{P \cdot u}{P \cdot q} \qquad\qquad z_{\mathbb{P}} \equiv \frac{q \cdot v}{q \cdot (P - p_Y)} \tag{5}$$

yield the fractions of the photon and pomeron momenta respectively carried by the partons involved in the hard interaction.

Hadron level cross sections are measured differentially in the estimators[1] $x_\gamma^{\rm jets}$ and $z_{\mathbb{P}}^{\rm jets}$ of the variables x_γ and $z_{\mathbb{P}}$. In the photoproduction analysis, the jet variables are defined as

$$x_\gamma^{\rm jets} \equiv \frac{\sum_{\rm jets}(E_i - p_{z,i})}{\sum_{\rm X}(E_i - p_{z,i})} \qquad\qquad z_{\mathbb{P}}^{\rm jets} \equiv \frac{\sum_{\rm jets}(E_i + p_{z,i})}{\sum_{\rm X}(E_i + p_{z,i})} \ , \tag{6}$$

[1] Throughout this paper, hadron level variables are represented with the superscripts `jet' or `jets' in order to distinguish them from parton level quantities.

where the sums labelled `jets' and `X' run over all hadrons attributed to the dijet system and to the full system X respectively. The hadron energies E_i and longitudinal momenta $p_{z,i}$ are calculated in the HERA laboratory frame, the positive z direction being that of the proton beam. In DIS, the relationship[2]

$$z_{\mathbb{P}}^{\text{jets}} \equiv \beta(1 + \frac{\hat{s}^{\text{jets}}}{Q^2}) \tag{7}$$

defines the hadron level variable, where

$$\hat{s}^{\text{jets}} \equiv (\sum_{\text{jets}} E_i)^2 - (\sum_{\text{jets}} \vec{p}_i)^2 . \tag{8}$$

3 Monte Carlo simulations

Monte Carlo simulations are used to correct the data for detector inefficiencies and for migrations of kinematic quantities due to the finite resolution of the reconstruction. For all events generated, the H1 detector response is simulated in detail and the Monte Carlo events are subjected to the same analysis chain as the data.

Hard diffractive scattering in photoproduction is modelled using the POMPYT 2.6 [33] simulation, which is a diffraction-specific extension to PYTHIA[34], containing both direct ($x_\gamma = 1$) and resolved ($x_\gamma < 1$) photon interactions. For DIS, the RAPGAP 2.02 [35] model is used. In both cases, a partonic sub-structure is ascribed to the pomeron. The diffractive contribution σ^{D} to the cross section takes the form

$$\mathrm{d}\sigma^{\text{D}}(ep \to epX) = f_{\mathbb{P}/\text{p}}(x_{\mathbb{P}}, t) \cdot \mathrm{d}\sigma^{e\mathbb{P}\to\text{eX}}(\mu, x_\gamma, z_{\mathbb{P}}) , \tag{9}$$

where $f_{\mathbb{P}/\text{p}}(x_{\mathbb{P}}, t)$ represents the pomeron flux associated with the beam proton and $\mathrm{d}\sigma^{e\mathbb{P}\to\text{eX}}(\mu, x_\gamma, z_{\mathbb{P}})$ is the cross section for the electron-pomeron hard interaction at a scale μ. In POMPYT, a flux $f_{\gamma/e}(y, Q^2)$ of transverse photons is factorised from the beam electron using the equivalent photon approximation [36], such that

$$\mathrm{d}\sigma^{e\mathbb{P}\to\text{eX}}(\mu, x_\gamma, z_{\mathbb{P}}) = f_{\gamma/e}(y, Q^2) \cdot \mathrm{d}\sigma^{\gamma\mathbb{P}\to\text{X}}(\mu, x_\gamma, z_{\mathbb{P}}) . \tag{10}$$

In both models, the pomeron flux factor is taken to be

$$f_{\mathbb{P}/\text{p}}(x_{\mathbb{P}}, t) = \left(\frac{1}{x_{\mathbb{P}}}\right)^{2\alpha_{\mathbb{P}}(t)-1} e^{b_{\mathbb{P}} t} , \tag{11}$$

with trajectory $\alpha_{\mathbb{P}}(t) = 1.20 + 0.26\,t$ and slope parameter $b_{\mathbb{P}} = 4.6\ \text{GeV}^{-2}$. This $x_{\mathbb{P}}$ dependence matches that extracted by H1 in a fit to $F_2^{D(3)}$ (fit B of [16]), the normalisation and t dependences being the same as those assumed in that fit. The t dependence is consistent with that recently measured in diffractive DIS by the ZEUS collaboration [11].

The electron-pomeron cross section, $\mathrm{d}\sigma^{e\mathbb{P}\to\text{eX}}(\mu, x_\gamma, z_{\mathbb{P}})$, is obtained from hard scattering matrix elements to leading order in QCD, convoluted with parton distributions for the pomeron at momentum fraction $z_{\mathbb{P}}$ and for the photon at momentum fraction x_γ. The scale μ at which

[2] This relationship is derived from equations (3 - 5) assuming that the photon interacts directly ($u = q$) and that the parton v entering the hard scattering is massless.

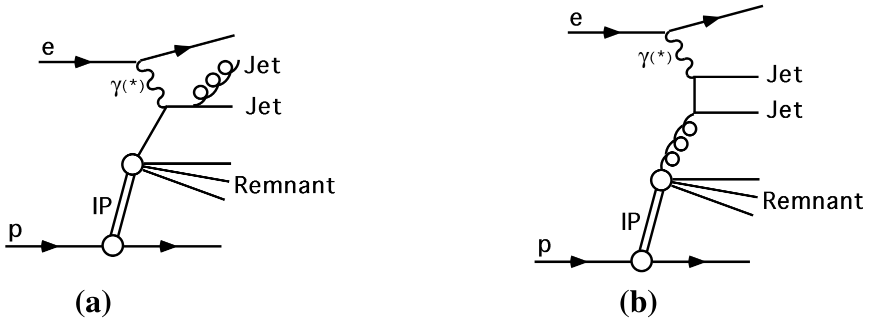

Figure 2: $\mathcal{O}(\alpha_{\mathrm{em}}\alpha_{\mathrm{s}})$ direct photon processes leading to diffractive dijet production. (a) Example QCD-Compton process; (b) Boson-Gluon Fusion.

the parton distributions are taken is chosen to be $\hat{p}_T$. In RAPGAP and for direct processes in POMPYT, the dominant high $\hat{p}_T$ process involving a quark from the exchange is the QCD-Compton mechanism $\gamma^{(*)}q \to qg$ (figure 2a), whereas it is the boson-gluon fusion process $\gamma^{(*)}g \to q\bar{q}$ (figure 2b) for a gluon from the exchange.

A set of pomeron parton distributions is implemented in the simulations that is dominated at low scales by a gluon distribution peaked at large z_{IP} [16]. For the resolved photon component in POMPYT, the parton distribution functions of the photon are taken from the leading order GRV parameterisation[37]. Outgoing charm quarks are generated through the photon-gluon and gluon-gluon fusion processes. Intrinsic transverse momentum of the incoming partons is simulated for the photon in POMPYT, but not for the pomeron in either model.

A small contribution from a sub-leading exchange (IR) is also included in the simulations, as has been found necessary in both photoproduction[12] and DIS[16]. As in the fits to inclusive large rapidity gap data, the flux factor has the same form as equation (11), with $\alpha_{\mathrm{IR}}(t) = 0.50 + 0.90\,t$ and $b_{\mathrm{IR}} = 2.0\ \mathrm{GeV}^{-2}$. The parton densities for the sub-leading exchange are taken from a parameterisation for the pion[38].

To avoid divergences in the calculation of QCD matrix elements for scattering from massless partons, a cut is applied at the generator level, $\hat{p}_T > 2\ \mathrm{GeV}$ (POMPYT) and $\hat{p}_T > \sqrt{2}\ \mathrm{GeV}$ (RAPGAP). The losses due to these cuts are negligible for jets with transverse momentum $p_T^{\mathrm{jet}} > 5\ \mathrm{GeV}$. Higher order effects in the QCD cascade are simulated using parton showers [39] in the leading $\log(\mu)$ approximation (MEPS). For systematic studies, the parton showering is replaced in RAPGAP by the colour dipole model (CDM) as implemented in ARIADNE [40]. Hadronisation is simulated in both models using the Lund string model [41].

As explained in section 5, Monte Carlo simulations are also used to compare the meas-ured hadron level cross sections with the predictions of theoretical models. Several sets of pomeron parton densities are implemented in the RAPGAP and POMPYT simulations for this purpose. Additional models based on the diffractive interaction of the $q\bar{q}$ fluctuation of the photon and on soft colour interactions in inclusive DIS are also tested.

4 Experimental procedure

The measurements presented here are based on H1 e^+p data[3] taken during 1994. An integrated luminosity of $2.24 \pm 0.03\ \mathrm{pb}^{-1}$ is used for the photoproduction analysis and $1.96 \pm 0.03\ \mathrm{pb}^{-1}$ for DIS. Detailed descriptions of the photoproduction and DIS measurements can be found in [42] and [43] respectively.

[3]The lepton beam particle is referred to in this paper as `the electron'.

4.1 The H1 detector and kinematic reconstruction

The H1 detector is described in detail elsewhere [44]. A brief account of the components that are most relevant to the present analyses is given here. The coordinate system convention for the experiment defines the forward, positive z direction as being that of the outgoing proton beam, corresponding to the region where pseudorapidity, $\eta = -\ln \tan \theta/2$, is positive.

A finely segmented electromagnetic and hadronic liquid argon calorimeter (LAr) provides smooth and hermetic coverage in the range $-1.5 \lesssim \eta \lesssim 3.4$ with energy resolution $\sigma(E)/E \simeq 0.11/\sqrt{E}$ for electromagnetic showers and $\sigma(E)/E \simeq 0.5/\sqrt{E}$ for hadrons (E in GeV) as measured in test beams. The Backward Electromagnetic lead scintillator Calorimeter (BEMC) covers the region $-3.4 \lesssim \eta \lesssim -1.4$ with resolution $\sigma(E)/E \simeq 0.10/\sqrt{E}$. Beam induced backgrounds are heavily suppressed using information from the Time of Flight scintillator (ToF), which is situated immediately backward of the BEMC. Charged track momenta are measured in the range $-1.5 \lesssim \eta \lesssim 1.5$ in the two large concentric drift chambers (CJC) of the central tracker, located inside a 1.15 T solenoidal magnetic field. Luminosity is measured by detecting electrons and photons from the bremsstrahlung process $ep \rightarrow ep\gamma$ in photon and electron crystal calorimeters situated at $z = -103$ m and $z = -33$ m respectively.

In the photoproduction analysis, the final state electron is detected in the electron tagger of the luminosity system (eTag), which has an acceptance such that $Q^2 < 10^{-2}$ GeV^2. The measurement of the scattered electron energy E'_e is used to reconstruct y according to $y = 1 - E'_e/E_e$, where $E_e = 27.5$ GeV is the electron beam energy.

In DIS, final state electrons at polar scattering angles $156° < \theta_e < 174°$ are identified using the BEMC in combination with a hit in multi-wire proportional chambers (BPC) mounted directly in front of it. The inclusive kinematic variables are calculated as

$$Q^2 = 4 E_e E'_e \cos^2 \frac{\theta_e}{2} \qquad y = 1 - \frac{E'_e}{E_e} \sin^2 \frac{\theta_e}{2} \qquad x = \frac{Q^2}{sy} \; , \tag{12}$$

using the measurements of E'_e in the BEMC and θ_e from the associated BPC hit in combination with the interaction vertex reconstructed in the central tracker.

The combined use of the Proton Remnant Tagger (PRT) scintillator surrounding the forward beampipe at $z = 24$ m, three drift chamber layers of the Forward Muon Detector (FMD) at $6 \lesssim z \lesssim 7$ m and the copper-silicon sandwich `plug' calorimeter nearest the beam-pipe at $z \simeq 5$ m provides sensitivity to hadronic energy flow at pseudorapidities up to $\eta \simeq 7.5$ [16, 12].

4.2 Large rapidity gap event selection

The trigger used to collect the photoproduction data was based on a scattered electron detected in the eTag and at least one track in the CJC. The DIS data were triggered on the basis of an energy cluster in the BEMC fulfilling the timing criteria of the ToF.

A number of selection criteria are applied in order to restrict the measurements to regions in which the acceptance is large and uniform and to suppress backgrounds. In both measurements, the reconstructed position of the event vertex is required to lie within 30 cm ($\sim 3\sigma$) of the mean interaction point in the z coordinate. In the photoproduction analysis, the scattered electron energy must correspond to the region $0.25 < y < 0.7$. To suppress the case in which a bremsstrahlung process is superimposed on a photoproduction event, the energy measured in the photon detector of the luminosity system is required to be less than $2\ \mathrm{GeV}$.

The DIS analysis is restricted to the region $7.5 < Q^2 < 80\ \mathrm{GeV}^2$ and $0.1 < y < 0.7$. Photoproduction events with high energy hadrons in the BEMC are removed from the DIS sample by imposing three conditions: the energy of the scattered electron E'_e must be greater than $8\ \mathrm{GeV}$, the radius of the electromagnetic cluster associated with the electron candidate must be less than $5\ \mathrm{cm}$ and there must be a BPC hit with a transverse distance of less than $5\ \mathrm{cm}$ from the centroid of the cluster. To suppress events with initial state electromagnetic radiation, the summed $E - p_z$ of all reconstructed particles including the electron is required to be greater than $40\ \mathrm{GeV}$.

Events with large forward rapidity gaps are selected in both analyses by demanding that there be no recorded signal above noise levels in the PRT, the FMD and the plug calorimeter. In addition, the most forward calorimeter cluster with a measured energy of 400 MeV or more must have $\eta < 3.2$. These selection criteria ensure that the forward limit of the system X is contained within the main detector components and the pseudorapidity gap separating X and Y spans at least the region $3.2 < \eta \lesssim 7.5$. The range of accessible masses of the system X is thus extended considerably compared to previous diffractive jet analyses at HERA[6, 7, 8]. The upper limit of the pseudorapidity gap restricts the measurements to the region $M_Y < 1.6\ \mathrm{GeV}$ and $|t| < 1.0\ \mathrm{GeV}^2$.

4.3 Invariant mass and jet reconstruction

The hadronic system X is detected and measured in the LAr and BEMC calorimeters together with the CJC. The mass M_X is reconstructed by combining tracks and calorimeter clusters in energy flow algorithms that avoid double counting [26, 12]. The invariant mass of X is then reconstructed according to

$$M_X^2 = (\sum_i E_i)^2 - (\sum_i \vec{p_i})^2 \ , \tag{13}$$

where the sums extend over all selected tracks and clusters. W^2 is reconstructed from the measurement of the final state electron in DIS and using $W^2 = s\,(E - p_z)_X /\ 2\,E_e$ in photoproduction. The remaining diffractive kinematic variables are computed using

$$x_{\mathbb{P}} = \frac{M_X^2 + Q^2}{W^2 + Q^2} \qquad\qquad \beta = \frac{Q^2}{M_X^2 + Q^2} \ , \tag{14}$$

where t and the proton mass squared are neglected. A cut of $x_{\mathbb{P}} < 0.05$ is applied to further reduce non-diffractive contributions. In the DIS analysis, the data are also restricted to $x_{\mathbb{P}} > 0.005$ to remove events in which the system X lies backward of the acceptance region of the LAr calorimeter.

The large rapidity gap samples are subjected to jet searches using a cone algorithm[45] (radius $\sqrt{\Delta\eta^2 + \Delta\phi^2} = 1$), applied to the tracks and clusters included in the reconstruction of M_X. The jet finding takes place in the rest frame of the system X (equivalently the $\gamma^{(*)}\mathbb{P}$ centre of mass frame), with transverse energies calculated relative to the $\gamma^{(*)}$ axis in that frame. In transforming to the rest frame of X, the value of $|t|$ is fixed at its minimum kinematically allowed value, such that $p_X = q + x_{\mathbb{P}} P$. In the photoproduction case, a simple Lorentz boost in the beam direction is thus required. For DIS, the beam and γ^* axes are not collinear.

Exactly two jets with transverse energy $E_T^{\rm jet} > 5$ GeV are required. To ensure that the bulk of the jet energy is restricted to the region covered by the LAr calorimeter, events are only considered if both jet axes lie within the region of laboratory pseudorapidity $-1.0 < \eta_{\rm lab}^{\rm jet} < 2.0$ (photoproduction) and $-1.0 < \eta_{\rm lab}^{\rm jet} < 2.2$ (DIS). After these requirements, 477 events remain in the photoproduction sample and 54 events remain for DIS.

The distribution of transverse energy flow about the jet axes for the photoproduction measurement is shown in figure 3. For the jet profile in $\Delta\phi$, activity throughout the full range of pseudorapity is included in the plot, which exhibits a clear back-to-back two jet structure. The r.m.s. of the distribution in azimuthal difference between the jet axes is approximately $25°$. For the jet profile in $\Delta\eta$, only transverse energy flow within one radian in azimuth of the jet axis is shown. The level of activity outside the jet cone is comparable to that for inclusive jet photoproduction in the backward region [46]. It is smaller in the forward region in the present data, due to the reduction in phase space available for underlying activity implied by the rapidity gap. The jet profiles in DIS show similar characteristics.

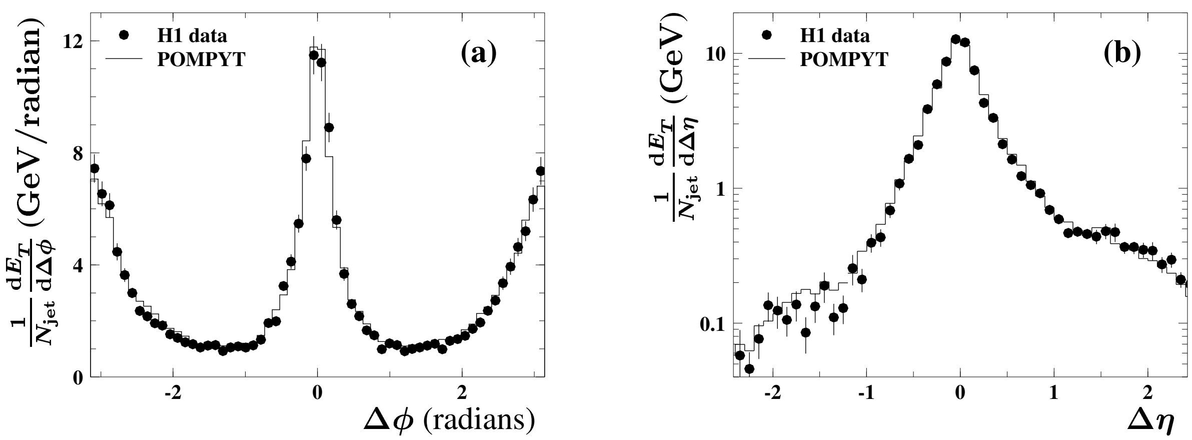

Figure 3: The observed distribution of transverse energy flow about the jet axis for the large rapidity gap photoproduction dijet sample. $\Delta\eta$ and $\Delta\phi$ are the distances from the jet axis in azimuthal angle and pseudorapidity respectively. (a) The jet profile in azimuth integrated over the full range of pseudorapidity. (b) The jet profile in pseudorapidity integrated over one radian of $\Delta\phi$ about the jet axis.

The additional dijet variables $\hat{s}^{\rm jets}$, $x_\gamma^{\rm jets}$ and $z_{I\!P}^{\rm jets}$ are reconstructed as specified in equations (6 – 8). The POMPYT and RAPGAP simulations have been used to investigate the correlations between the hadron jets that define the measured cross sections and the underlying parton dynamics. The hadronisation process results in only a small smearing of the jet directions relative to those of the outgoing partons, with r.m.s. shifts of approximately 0.13 pseudorapidity units and $6°$ in azimuth. The smearing effects due to hadronisation are stronger for p_T, x_γ and $z_{I\!P}$, leading to a resolution of approximately 20%, except near $x_\gamma = 1$ and $z_{I\!P} = 1$, where events are smeared at the hadron level throughout the regions $x_\gamma^{\rm jets} \gtrsim 0.6$ and $z_{I\!P}^{\rm jets} \gtrsim 0.6$.

4.4 Cross section measurement

The cross sections presented here are defined solely in terms of ranges in kinematic variables and jet criteria. They are corrected to the Born level. The kinematic domains to which the cross section measurements are corrected are summarised in table 1. The photoproduction cross sections are defined in terms of a laboratory pseudorapidity region for the jets. In the DIS measurement, the y and $x_{I\!P}$ restrictions imply a similar range of pseudorapidity. No attempt is made to unfold to parton cross sections or to a specific physics process such as diffraction, due to the large uncertainties inherent in such a procedure.

PHOTOPRODUCTION	DIS
$Q^2 < 0.01\ \mathrm{GeV}^2$	$7.5 < Q^2 < 80\ \mathrm{GeV}^2$
$0.25 < y < 0.7$	$0.1 < y < 0.7$
$x_{I\!P} < 0.05$	$0.005 < x_{I\!P} < 0.05$
$M_Y < 1.6\ \mathrm{GeV}$	
$\|t\| < 1.0\ \mathrm{GeV}^2$	
Exactly two jets with $p_T^{\mathrm{jet}} > 5\ \mathrm{GeV}$	
$-1 < \eta_{\mathrm{lab}}^{\mathrm{jet}} < 2$	

Table 1: The kinematic domains in which the photoproduction and DIS cross sections for the process $ep \to eXY$ are measured.

The data are corrected for detector inefficiencies and migrations of kinematic quantities in the reconstruction using the POMPYT (photoproduction) and RAPGAP (DIS) Monte Carlo models as described in section 3. For both measurements, these simulations give an adequate description of all relevant reconstructed data distributions. Migrations about the upper $x_{I\!P}$ boundary of the measurements are evaluated with the additional use of the PYTHIA [34] model in photoproduction and the DJANGO [47] model in DIS. Migrations about the limits of the measurements in M_Y are studied using the PHOJET [48] and PYTHIA models of soft photoproduction and the DIFFVM [49] simulation of vector meson electroproduction. Each of these models contains diffractive events both where the proton remains intact and where it dissociates. For the data points presented, the lowest overall acceptance is 37% and the lowest bin purity[4] is 32% according to the simulations.

Fluctuations in the level of noise in the forward detector components, resulting in the rejection of events within the kinematic range of the measurements, are studied using a sample of events which were triggered randomly throughout the run period in which the data were collected. A correction of $(6.1 \pm 2.0)\%$ is applied. The expected background from the process $\gamma\gamma \to q\bar{q}$ has been quantified using the LPAIR Monte Carlo model [50]. Subtractions of 1.7 ± 0.3 events in the photoproduction analysis and 0.7 ± 0.1 events for DIS are made, concentrated at large $z_{I\!P}^{\mathrm{jets}}$ in both cases. A correction of 1.8% is applied in the photoproduction measurement to account for the loss of signal due to the removal of events in which a bremsstrahlung process is overlaid. Photoproduction background to the DIS measurement has been found to be less than 1.4% using the POMPYT simulation. Beam induced backgrounds are found to be negligible in both data samples.

QED radiative corrections have been shown to be small in previous photoproduction measurements [51] due to the cut on the energy in the photon detector. They are neglected here. Radiative corrections to the DIS measurement are evaluated using the RAPGAP Monte Carlo model interfaced to the program HERACLES [52]. Corrections of up to 10% are applied.

[4] Purity is defined as the proportion of the simulated events reconstructed in an interval that were also generated in that interval.

4.5 Systematic error analysis

The largest contributions to the systematic errors in both measurements arise from uncertainties in detector calibration.

- A 4% uncertainty in the absolute hadronic energy scale of the LAr and a 3% uncertainty in the fraction of energy carried by tracks are reflected in the determination of jet transverse momenta. Together with a 20% hadronic energy scale uncertainty of the BEMC, these uncertainties also affect the measurement of $x_{\mathbb{P}}$. The effects on the photoproduction and DIS measurements are different, mainly because of the different algorithms used for the selection of tracks and clusters. In photoproduction, the combined uncertainty due to the LAr, BEMC and track scales is approximately 20% in the cross sections differential in $\eta_{\rm lab}^{\rm jet}$ and $p_T^{\rm jet}$ and approximately 15% for the $x_\gamma^{\rm jets}$ and $z_{\mathbb{P}}^{\rm jets}$ distributions. These errors arise predominantly from the LAr and are strongly correlated between data points. For the DIS measurement, the LAr and track uncertainties both result in large contributions to the systematic errors. Together with the BEMC uncertainty, their net result is an uncertainty at the level of 15% on the measurements, which is less strongly correlated between data points.
- In photoproduction, a 5% systematic error arises from the uncertainty in the eTag acceptance averaged over the y range of the measurement. The efficiency of the CJC component of the trigger is known to 4.5% from studies using an independent trigger.
- In the DIS measurement there is a 1% uncertainty in the scattered electron energy E'_e and a $1\ \mathrm{mrad}$ uncertainty on the electron scattering angle θ_e. These affect the determination of the $\gamma^*\mathbb{P}$ collision axis and give rise to further uncertainties in the cross sections of 6% and 2% on average respectively.
- Uncertainties of 20% in the PRT efficiency and 30% in the plug energy scale result in normalisation uncertainties of 4% and 2% of the measured cross sections respectively.
- The uncertainty in the luminosity of the data samples is 1.5%.

Additional systematic errors arising from the uncertainties in the acceptance and mig-ration corrections are estimated by repeating the measurements with variations in the kinematic dependences and other details of the Monte Carlo models.

- The uncertainties arising from the shapes of the $p_T^{\rm jet}$ and $z_{\mathbb{P}}^{\rm jets}$ distributions in the models are studied by changing the simulated distributions by amounts that are larger than the final errors on the measurements presented here. The overall transverse momentum distributions are reweighted by $(1/\hat{p}_T)^{\pm 1}$, resulting in average uncertainties of 7% in the photoproduction measurement and 5% for DIS. The overall momentum distribution of the partons in the pomeron is reweighted by $z_{\mathbb{P}}^{\pm 0.2}$ and $(1 - z_{\mathbb{P}})^{\pm 0.2}$ for photoproduction, leading to an average uncertainty of 1% in the measured cross sections. In the DIS case, where the $z_{\mathbb{P}}$ distribution is less well constrained by the present data, factors of $z_{\mathbb{P}}^{\pm 0.5}$ and $(1 - z_{\mathbb{P}})^{\pm 0.5}$ are applied, leading to an average uncertainty of 5%. The ratio of resolved to direct processes is also varied by 50% in the POMPYT simulation, giving rise to an uncertainty of 2% on average in the photoproduction measurement.

- The $x_{\mathbb{P}}$ and t distributions are varied by factors chosen to result in changes that are larger than the level of precision determined by more inclusive measurements. Reweighting the simulated distributions by $(1/x_{\mathbb{P}})^{\pm 0.2}$ [12, 16] leads to uncertainties of 1% in the measured cross sections on average. The mean uncertainty from varying the t distribution by factors $e^{\pm 2t}$ [11] is 3%.

- The number of events in the Monte Carlo models that migrate into the sample from the unmeasured region $x_{\mathbb{P}} > 0.05$ is varied by $\pm 50\%$, leading to a mean uncertainty of 6% in the photoproduction cross sections and 7% in DIS.

- A total error of 6% in the measured cross sections accounts for uncertainties in the migrations across the boundary $M_Y < 1.6$ GeV. This error is estimated using the Monte Carlo models that include proton dissociative processes. The M_Y distributions, the ratio of single to double dissociation cross sections and the fragmentation scheme for proton dissociation are varied in the models in the manner described in [12, 16].

- Uncertainties due to the modelling of hadronisation are estimated from the difference between the results obtained in the DIS analysis using the colour dipole and the parton showering simulations. These errors are at the level of 3% of the measured cross sections.

In the photoproduction measurement, the dominant source of error is the hadronic energy scale of the LAr. In DIS, the statistical errors are dominant.

5 Results and discussion

In this section, differential cross sections are presented for dijet production in the photoproduction and DIS kinematic regions specified in table 1. The results are given in figures 4 – 6 and table 2. In all figures, the inner error bars show the statistical errors and the outer error bars show the statistical errors added in quadrature with those systematic uncertainties that vary from data point to data point. The shaded bands show overall normalisation uncertainties, which contain contributions from the LAr, BEMC and tracker scale calibrations in the photoproduction case.

The data are compared with models of hard diffraction using the POMPYT and RAPGAP simulations described in section 3. For the pomeron, three sets of light quark and gluon distributions are implemented in the Monte Carlo generators at a scale $\mu = \hat{p}_T$ for comparisons with the measurements. These correspond to the results of leading order DGLAP fits to the H1 measurement of $F_2^{D(3)}$ (section 6 of [16]). The first set of parton distributions (labelled `F_2^D fit 1' in the figures) is obtained from a fit in which only quarks contribute to the pomeron structure at the starting scale $\mu_0^2 = 3\ \mathrm{GeV}^2$. This set does not give a good description of $F_2^{D(3)}$ and is used here only to illustrate the sensitivity of the measurement to the partonic structure of the interaction. In two further fits, gluons are introduced at the starting scale in addition to quarks. Both of these fits give an acceptable description of $F_2^{D(3)}$ and in both cases, the fraction of the pomeron momentum carried by gluons is between 80% and 90% for $4.5 < \mu^2 < 75\ \mathrm{GeV}^2$. These two fits differ in the parameterisation used for the parton densities such that the gluon distribution at low scales is either relatively flat in $z_{\mathbb{P}}$ (labelled `$F_2^D$ fit 2') or is peaked in the region of large $z_{\mathbb{P}}$ (labelled `F_2^D fit 3'). They are hereafter referred to as the `flat' and `peaked' gluon solutions respectively.

A sub-leading exchange is included for all three sets of parton distributions in the manner described in [16]. The resulting predicted contribution is between 10% and 20% of the measured cross section in all photoproduction and DIS simulations (see figure 4).

A measure of the theoretical uncertainties in the predictions of the models is obtained by varying the details of the simulations. When the CDM scheme is used in place of parton showering in RAPGAP, the predicted dijet rate increases by approximately 25%. Taking $\mu = \hat{p}_T/2$ or $2\hat{p}_T$ in either POMPYT or RAPGAP alters the predictions at the level of 20%. Taking the LAC-1 [53] parameterisation of the photon parton distributions [5] in POMPYT in place of GRV changes the predictions by up to 10%. Interference between the pomeron and sub-leading exchanges was found to be possible in [12, 16], but is not considered here. Higher order corrections to the models beyond those already simulated by parton showering may also alter the predicted cross sections, though their effects have been found to be small in inclusive dijet production [54].

5.1 Jet rates and transverse momentum dependence

Figures 4a and b show the photoproduction and DIS cross sections differential in the jet momentum p_T^{jet} transverse to the $\gamma^{(*)}\mathbb{P}$ interaction axis. In the $x_{\mathbb{P}}$ region of the present data, the total mass of the hadronic system containing the jets ($M_X \lesssim 40$ GeV) does not greatly exceed the minimum accessible value for $p_T^{\text{jet}} > 5$ GeV of $M_X = 10$ GeV. The p_T^{jet} distributions therefore reflect phase space limitations in addition to dynamics. They are discussed here solely in terms of comparisons with the POMPYT and RAPGAP simulations.

The models in which the diffractive parton distributions consist solely of quarks at the starting scale underestimate the photoproduction and DIS differential cross sections by factors varying between 3 and 6. The models in which the diffractive parton distributions are dominated by hard gluons are much closer to the data, confirming the conclusions of other HERA diffractive analyses [14, 16, 7, 8, 26, 27, 28, 55] that a large gluon component is required in the pomeron parton distributions. The successful description of the dijet cross sections by the hard gluon models lends support to the concept of factorisable pomeron parton distributions, appropriate for the modelling of diffractive interactions with hard scales other than Q.

The sensitivity of dijet rates to the partonic composition of the pomeron can be understood phenomenologically in terms of the hard interactions that can be initiated by a quark or a gluon. If the diffractive parton distributions are quark dominated, then the bulk of the diffractive DIS cross section is expected to correspond to the $\mathcal{O}(\alpha_{\text{em}})$ process $\gamma^* q \to q$ (figure 2a without the emission of a gluon in the hard process) and the resulting system X must be highly aligned with the $\gamma^*\mathbb{P}$ axis[18]. The QCD-Compton mechanism (figure 2a), which yields high $\hat{p}_T$ outgoing partons, is suppressed relative to lowest order by $\mathcal{O}(\alpha_{\text{s}})$. By contrast, for a gluon dominated exchange the lowest order process available is boson-gluon fusion (figure 2b), yielding two outgoing partons which can have large $\hat{p}_T$ due to the virtuality of the quark propagator. Given that the overall normalisation of the product of the pomeron flux and parton distributions is constrained in the simulations by the measurement of $F_2^{D(3)}$ [16], a gluon dominated exchange is thus expected to result in significantly more copious high p_T dijet electroproduction than a quark dominated exchange. Similar arguments lead to the same conclusions for direct photoproduction. In resolved photoproduction, the differences between

[5] The LAC-1 parameterisation has a larger gluon content than the GRV parameterisation.

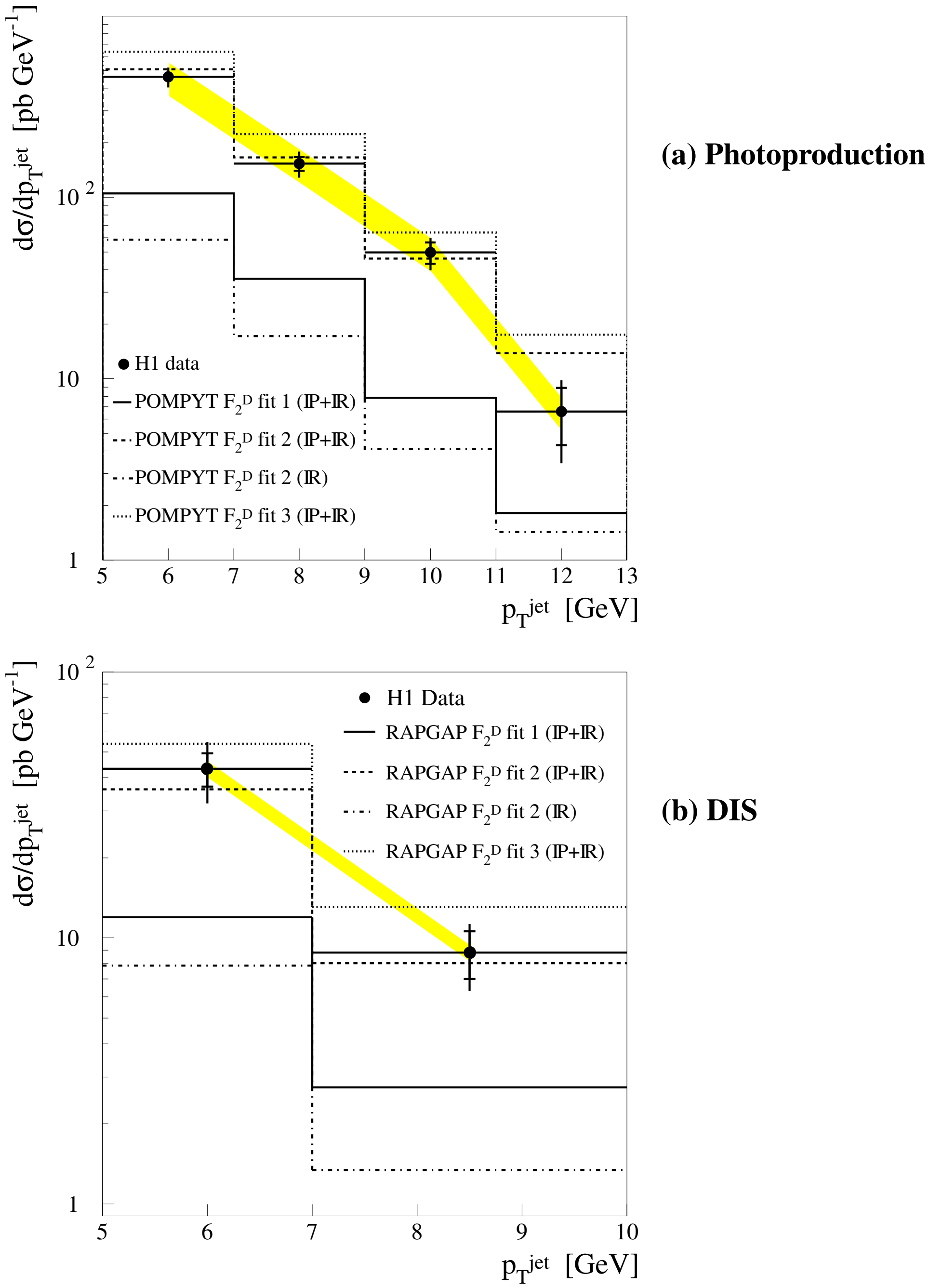

Figure 4: Differential cross sections in the component of the jet momentum transverse to the $\gamma^{(*)}\mathbb{P}$ collision axis in the rest frame of X for the process $ep \to eXY$ where X contains two jets. (a) Photoproduction and (b) DIS cross sections measured in the kinematic regions specified in table 1. There is one entry in the plots per jet. The shaded bands show the overall normalisation uncertainties. The data are compared to the predictions of the POMPYT (photoproduction) and RAPGAP (DIS) Monte Carlo models with three sets of leading order pomeron ($\mathbb{P}$) and meson ($\mathbb{R}$) parton distributions at a scale set by $\hat{p}_T$: quarks only (labelled F_2^D fit 1), `flat' gluon dominated (labelled $F_2^D$ fit 2) and `peaked' gluon dominated (labelled F_2^D fit 3) parton distributions at $\hat{p}_T^2 = 3$ GeV^2 (see [16]). The meson component of the `flat' gluon model is also shown.

the predictions for a quark and a gluon dominated exchange arise from the gluon : quark colour factor of $9:4$ and other details of quark and gluon induced matrix elements.

Comparing the data to the hard gluon simulations in more detail, the `flat' gluon model reproduces the overall dijet rates to well within the uncertainties. In both photoproduction and DIS, the `peaked' gluon model yields predictions that lie above the data (see also figures 5 and 6). Assuming that the model based on factorisable evolving diffractive parton distributions is valid, the measurements therefore tend to favour the `flat' gluon solution, though in light of the large experimental and theoretical uncertainties, no firm conclusions can be drawn.

5.2 Photoproduction and rapidity gap survival probability

The photoproduction cross section differential in jet pseudorapidity in the laboratory frame, $\mathrm{d}\sigma/\mathrm{d}\eta_{\mathrm{lab}}^{\mathrm{jet}}$ is shown in figure 5a. The $\eta_{\mathrm{lab}}^{\mathrm{jet}}$ distribution is sensitive to the decomposition of the data in the variables $x_{\gamma}^{\mathrm{jets}}$ and $z_{\mathrm{IP}}^{\mathrm{jets}}$, with the more forward region corresponding broadly to small x_{γ} and large z_{IP} processes. Both hard gluon dominated models acceptably reproduce the shape of the $\eta_{\mathrm{lab}}^{\mathrm{jet}}$ distribution, though the `flat' gluon solution is closer in normalisation.

Figure 5b shows the photoproduction cross section differential in $x_{\gamma}^{\mathrm{jets}}$. The contribution in the POMPYT simulation from true direct photon processes ($x_{\gamma}=1$) is peaked at the largest $x_{\gamma}^{\mathrm{jets}}$, though there are significant contributions throughout the region $x_{\gamma}^{\mathrm{jets}} \gtrsim 0.6$. It is clear from the measured distribution that both direct and resolved photon processes are present in the photoproduction data.

In inclusive jet photoproduction, soft interactions between spectator partons in the spatially extended photon and the proton, in addition to the hard interaction, have been found to be present in resolved photon processes [56]. In the diffractive case, multiple interactions would be expected to destroy rapidity gaps, an effect which has been parameterised in terms of a `survival probability' $S$ [29] and which would represent a breaking of diffractive factorisation. Since no full calculations of spectator interactions for diffractive photoproduction exist, we follow [57] and apply a constant weighting factor $\langle S\rangle = 0.75$ to all events in the POMPYT `flat' gluon model that are generated with $x_{\gamma} < 0.8$. This is a simplistic model, the 75% survival probability being an *a posteriori* choice. Figures 5b and 6a show the effects of the rapidity gap destruction model on the predicted photoproduction cross sections differential in $x_{\gamma}^{\mathrm{jets}}$ and $z_{\mathrm{IP}}^{\mathrm{jets}}$. The data can be described by the `flat' gluon model whether the survival probability is introduced or not. The same conclusion is reached when the $z_{\mathrm{IP}}^{\mathrm{jets}}$ distribution is measured separately in the two regions $x_{\gamma}^{\mathrm{jets}} < 0.8$ and $x_{\gamma}^{\mathrm{jets}} > 0.8$ (not shown). When rapidity gap destruction effects are considered for the `peaked' gluon solution, a survival probability $\langle S\rangle \sim 0.45$ gives a good description of the photoproduction data, though spectator interactions cannot explain the excess in the predictions of this model at large $z_{\mathrm{IP}}^{\mathrm{jets}}$ in DIS (figure 6b).

Studies of diffractive dijet production at the Tevatron suggest a breaking of diffractive factorisation [5]. From comparisons of the Tevatron data with models based on pomeron parton distributions extracted from diffractive DIS, there are indications that the rapidity gap survival probability may be as small as 0.1 for $p\bar{p}$ interactions at $\sqrt{s} = 1800\ \mathrm{GeV}$ [58]. Within models based on a pomeron with evolving partonic structure, there is thus evidence that any breaking of diffractive factorisation in the present resolved photoproduction data is weaker than that in $p\bar{p}$ data at larger centre of mass energy. A similar difference between resolved photoproduction at $W \sim 200\ \mathrm{GeV}$ and $p\bar{p}$ interactions at $\sqrt{s} = 1800\ \mathrm{GeV}$ is observed in the fraction of dijet events in which there is a rapidity gap between the jets [59]. The Tevatron data also suggest that

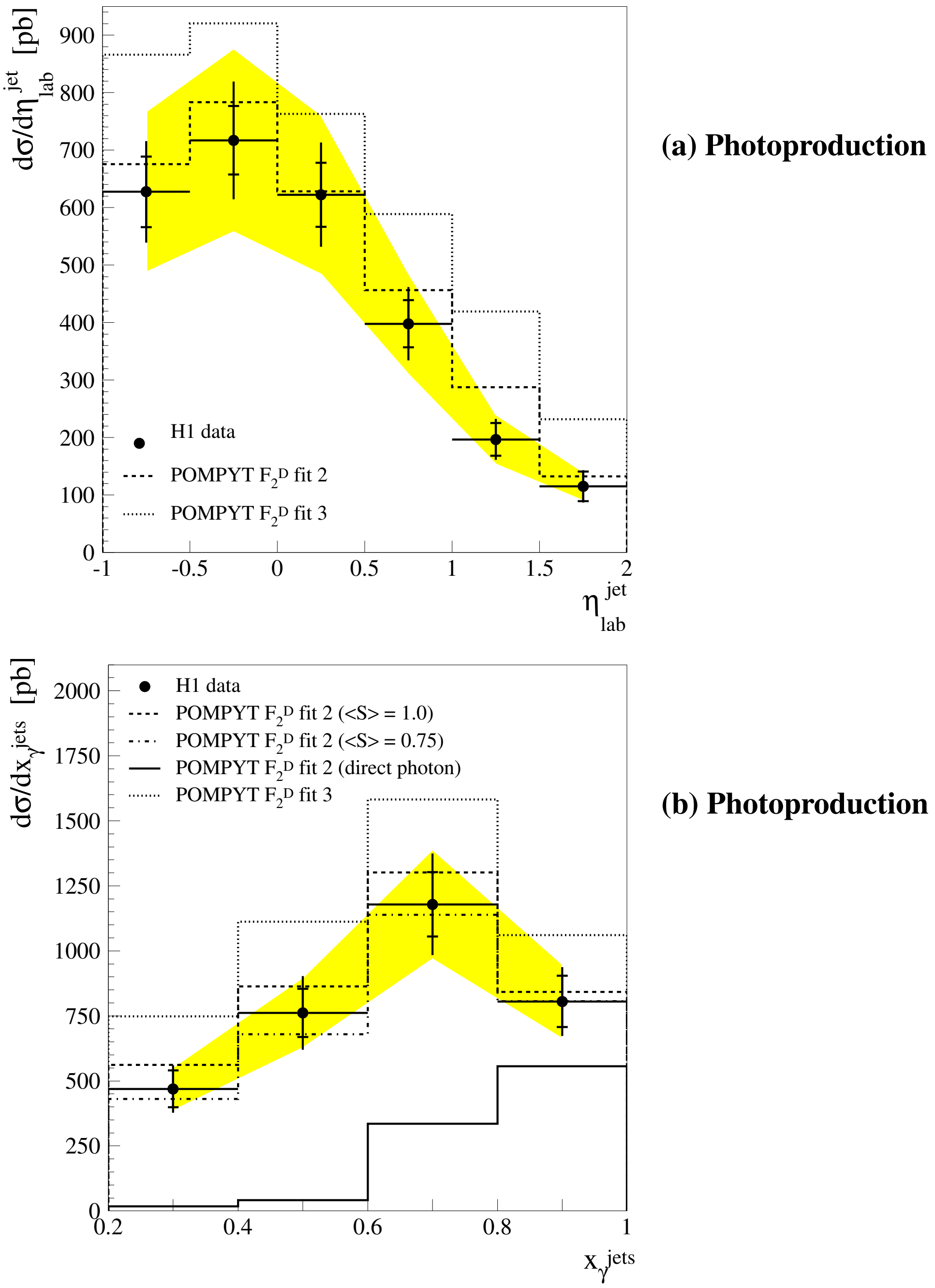

Figure 5: Differential cross sections for the production of two jets in the component X of the process $ep \to eXY$ in the photoproduction kinematic region specified in table 1. (a) The cross section differential in pseudorapidity in the HERA laboratory frame with one entry per jet. (b) The cross section differential in x_γ^{jets} with one entry per event. The shaded bands show the overall normalisation uncertainties. The data are compared to the predictions of the POMPYT Monte Carlo model with leading order pomeron parton densities at a scale set by $\hat{p}_T$ that are dominated by a `flat' (labelled $F_2^D$ fit 2) and a `peaked' (labelled F_2^D fit 3) gluon distribution at $\hat{p}_T^2 = 3$ GeV^2 (see [16]). In (b), the predictions for the `flat' gluon model are also shown with a rapidity gap survival probability of 0.75 applied to events with $x_\gamma < 0.8$. The contribution to the model from true direct ($x_\gamma = 1$) photon processes is also shown.

this fraction is smaller at $\sqrt{s} = 1800$ GeV than at $\sqrt{s} = 630$ GeV [5, 59]. Data from HERA and the Tevatron on dijet production in diffractive dissociation and on rapidity gaps between jets therefore both support the hypothesis that rapidity gap survival probabilities decrease with increasing centre of mass energy [30]

In [8], the ZEUS collaboration presented diffractive dijet photoproduction cross sections measured in a different kinematic region to that studied here. In particular, the range of $x_{\mathbb{P}}$ accessed is larger in the present measurement, resulting in an improved coverage of the low $x_\gamma^{\rm jets}$ and $z_{\mathbb{P}}^{\rm jets}$ regions. The `flat' gluon model derived from the H1 F_2^D measurements, as implemented in the POMPYT model, is found to be compatible with the ZEUS measurements in the specified kinematic domain when the survival probability $\langle S \rangle = 1$.

5.3 Dependence on fractional momentum from the pomeron

The photoproduction and DIS dijet production cross sections differential in $z_{\mathbb{P}}^{\rm jets}$ are presented and compared to Monte Carlo predictions in figures 6a and 6b respectively. In both kinematic regions, there are significant contributions at the largest $z_{\mathbb{P}}^{\rm jets}$ and the differential cross sections increase as $z_{\mathbb{P}}^{\rm jets}$ decreases.

The calculation by Bartels et al. [21] for the $q\bar{q}$ Fock state arising from transversely polarised photons is compared to the DIS data via the RAPGAP simulation in figure 6b. In the picture based on partonic fluctuations of the photon, this contribution is expected to be the dominant feature of diffractive DIS only at small $\hat{p}_T$ and for β values of around 0.5, larger than those typical of the present sample [25]. The diffractive interaction is modelled by coupling two gluons in a net colour singlet configuration to the outgoing quarks in all possible combinations. The calculation is performed in the double logarithmic approximation at $t = 0$, such that the cross section is closely related to the squared gluon distribution of the proton with momentum fraction $x = x_{\mathbb{P}}$ at a squared scale $\hat{p}_T^2 \cdot (Q^2 + M_X^2)/M_X^2$. The t dependence is modelled using a parameterisation of the proton form factor [60]. At the largest $z_{\mathbb{P}}^{\rm jets}$, where the full momentum of the system X is carried by the two jets, the prediction for the $q\bar{q}$ fluctuation alone is compatible with the data, given the large experimental uncertainties. At smaller $z_{\mathbb{P}}^{\rm jets}$, this model falls well short of the data. Fock states with higher parton multiplicities than $q\bar{q}$ are presumably dominant in the kinematic regime studied here, as has also been shown at large M_X and p_T in previous hadronic final state analyses [26, 27, 28]. No direct comparisons have been made with models of higher multiplicity photon fluctuations, though the scattering of the $q\bar{q}g$ Fock state where the gluon is the low transverse momentum parton has been identified with the boson-gluon fusion hard process [61].

Certain classes of non-factorising processes which may be present in resolved photoproduction are predicted to yield a `super-hard' contribution to diffraction for which $z_{\mathbb{P}} \equiv 1$ [31]. There is some experimental evidence for such a contribution from the UA8 collaboration [4], at the level of 30% of the data. The RAPGAP $q\bar{q}$ Fock state prediction ($z_{\mathbb{P}} \equiv 1$) illustrates that a `super-hard' contribution is expected to appear in the jet cross sections as a broad distribution with $z_{\mathbb{P}}^{\rm jets} \gtrsim 0.6$. This shape contrasts with that observed in both the photoproduction and the DIS data, where there are large contributions at $z_{\mathbb{P}}^{\rm jets} \lesssim 0.6$. `Super-hard' diffractive dijet production is therefore not the dominant feature of the present data, though it is expected to become increasingly visible as $|t|$ increases [31]. The UA8 measurements were for $1 \lesssim |t| \lesssim 2$ GeV^2, whereas $|t| < 1$ GeV^2 for the data presented here.

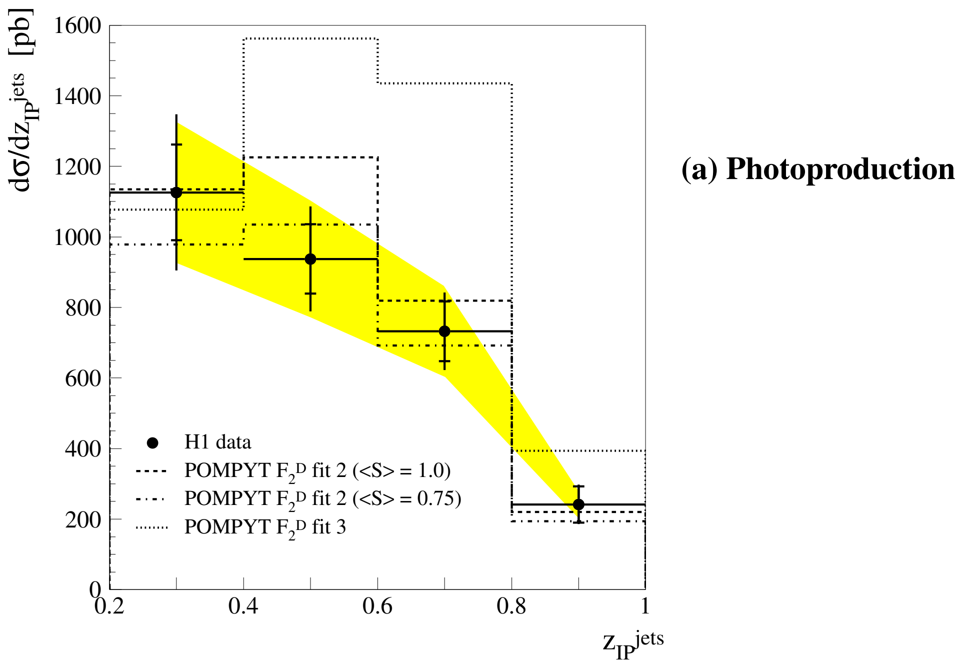

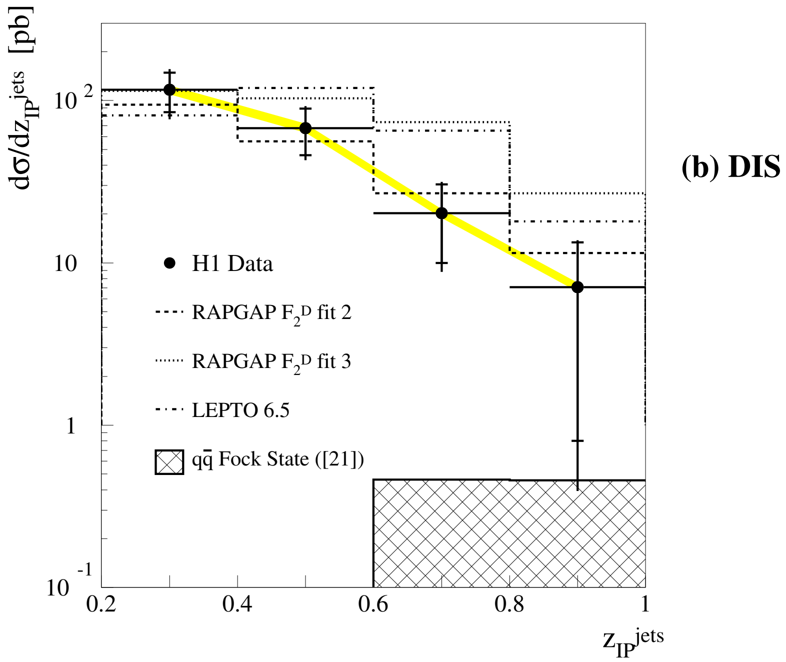

Figure 6: Differential cross sections in $z_{\mathbb{P}}^{\text{jets}}$ for the production of two jets in the component X of the process $ep \to eXY$. (a) Photoproduction and (b) DIS cross sections measured in the kinematic regions specified in table 1. The shaded bands show the overall normalisation uncertainties. The data are compared to the predictions of the POMPYT (photoproduction) and RAPGAP (DIS) Monte Carlo models with leading order parton densities for the pomeron at a scale set by $\hat{p}_T$ that are dominated by a `flat' (labelled $F_2^D$ fit 2) and a `peaked' (labelled F_2^D fit 3) gluon distribution at $\hat{p}_T^2 = 3$ GeV^2 (see [16]). In (a), the prediction of POMPYT for the `flat' gluon is also shown with a rapidity gap survival probability of 0.75 applied to events with $x_\gamma < 0.8$. Also shown in (b) are the RAPGAP implementation of a calculation [21] of the diffractive scattering of the $q\bar{q}$ fluctuation of the photon and the LEPTO 6.5 model with a probability of 0.5 for soft colour interactions to take place.

The DIS data are also compared with the LEPTO 6.5 [62] model of inclusive DIS in figure 6b. In this model, leading order hard interactions are convoluted with parton distributions for the proton, boson-gluon fusion being the dominant process in the low x region corresponding to the diffractive data. Soft interactions between the outgoing partons alter the final state colour connections without affecting the parton momenta, hence giving rise to large rapidity gaps [32]. The LEPTO model is able to reproduce the overall dijet production rate when the probability for soft colour interactions is around 0.5. The description of the shapes of the $p_T^{\rm jet}$ and $z_{I\!P}^{\rm jets}$ distributions is similar in quality to that of the RAPGAP `peaked' gluon model.

6 Summary

Cross sections have been measured for the production of two jets as components of the dissociating photon system X in the process $ep \rightarrow eXY$ ($M_Y < 1.6$ GeV, $|t| < 1$ GeV^2). A cone algorithm was used in the rest frame of X, requiring $p_T^{\rm jet} > 5$ GeV relative to the photon direction in that frame. Photoproduction cross sections have been measured differentially in $p_T^{\rm jet}$, $\eta_{\rm lab}^{\rm jet}$, $x_\gamma^{\rm jets}$ and $z_{I\!P}^{\rm jets}$, with clear evidence for the presence of resolved as well as direct photon processes. Diffractive dijet production has also been studied in DIS, with cross sections measured differentially in $p_T^{\rm jet}$ and $z_{I\!P}^{\rm jets}$ for the region $7.5 < Q^2 < 80$ GeV^2.

The measured dijet production rates and kinematic distributions have been compared to models of inelastic $eI\!P$ scattering in which diffractive parton densities, extracted from a measurement of inclusive diffractive DIS, are evolved using the DGLAP equations to the scale $\hat{p}_T$. Since $\hat{p}_T$ rather than Q was chosen for the scale of the hard interaction here, with $\hat{p}_T^2 \gg Q^2$ for most of the data, this represents a largely independent investigation of the validity of diffractive parton distributions for the description of both deep-inelastic and photoproduction interactions.

The dijet measurements can be described by models containing diffractive parton distributions that are dominated by hard gluons at low scales. For comparison, quark dominated diffractive parton densities result in dijet rates that are significantly smaller than those measured. Parton distributions in which the pomeron gluon structure is relatively flat as a function of $z_{I\!P}$ at low scales (fit 2 of [16]) describe the data better than those in which the gluon distribution is peaked at large $z_{I\!P}$ (fit 3 of [16]). There is no significant evidence for diffractive factorisation breaking due to spectator interactions where there is a photon remnant system. However, within the picture based on a pomeron with evolving partonic structure, a rapidity gap survival probability of around 0.75 cannot be excluded for the `flat' gluon solution. The photoproduction data are also compatible with the `peaked' gluon solution when the survival probability is around 0.45. The rapidity gap survival probability for resolved photoproduction at HERA is thus larger than that for $p\bar{p}$ interactions at higher energies at the Tevatron. There is no evidence for a large `super-hard' pomeron contribution for which $z_{I\!P} \equiv 1$.

When considered in terms of the diffractive scattering of partonic fluctuations of the virtual photon, the measured dijet rates in DIS cannot be described by a simulation of the $q\bar{q}$ Fock state alone. Fluctuations to states containing one or more gluons are therefore expected to be dominant in the high $\hat{p}_T$ and high M_X region investigated here.

The soft colour interaction mechanism, as implemented in the LEPTO Monte Carlo model, gives an acceptable description of the DIS data when the probability for rearrangements in the colour connections between outgoing partons is in the region of 0.5.

It has now been shown from inclusive diffractive cross section measurements, charged particle distributions and multiplicities, energy flow, event shapes and dijet cross sections that HERA diffractive data are consistently described by models that assume a t channel exchange with gluon dominated parton distributions, evolving with the scale of the hard interaction.

Acknowledgements

We are grateful to the HERA machine group whose outstanding efforts have made and continue to make this experiment possible. We thank the engineers and technicians for their work constructing and now maintaining the H1 detector, our funding agencies for financial support, the DESY technical staff for continual assistance and the DESY directorate for the hospitality which they extend to the non-DESY members of the collaboration. We have benefited from interesting discussions with J. Bartels and R. Engel.

References

[1] A. Kaidalov, Phys. Rep. **50** (1979) 157.
G. Alberi, G. Goggi, Phys. Rep. **74** (1981) 1.
K. Goulianos, Phys. Rep. **101** (1983) 169.
N. Zotov, V. Tsarev, Sov. Phys. Usp. **31** (1988) 119.

[2] G. Ingelman, P. Schlein, Phys. Lett. **B152** (1985) 256.
A. Donnachie, P. Landshoff, Phys. Lett. **B191** (1987) 309.
A. Donnachie, P. Landshoff, Nucl. Phys. **B303** (1988) 634.

[3] UA8 Collaboration, R. Bonino et al., Phys. Lett. **B211** (1988) 239.

[4] UA8 Collaboration, A. Brandt et al., Phys. Lett. **B297** (1992) 417.

[5] CDF Collaboration, F. Abe et al., Phys. Rev. Lett. **79** (1997) 2636.
K. Borras (CDF Collaboration), P. Rubinov (D0 Collaboration), to appear in Proc. of the 6th International Workshop on DIS and QCD, Brussels, Belgium, April 1998.

[6] H1 Collaboration, T. Ahmed et al., Nucl. Phys. **B435** (1995) 3.

[7] ZEUS Collaboration, M. Derrick et al., Phys. Lett. **B346** (1995) 399.
ZEUS Collaboration, M. Derrick et al., Phys. Lett. **B356** (1995) 129.

[8] ZEUS Collaboration, J. Breitweg et al., DESY 98-045, to appear in Eur. Phys. J.

[9] ZEUS Collaboration, M. Derrick et al., Phys. Lett. **B315** (1993) 481.

[10] H1 Collaboration, T. Ahmed et al., Nucl. Phys. **B429** (1994) 477.

[11] ZEUS Collaboration, J. Breitweg et al., Eur. Phys. J. **C1** (1998) 81.
ZEUS Collaboration, J. Breitweg et al., Eur. Phys. J. **C2** (1998) 237.

[12] H1 Collaboration, C. Adloff et al., Z. Phys. **C74** (1997) 221.

[13] ZEUS Collaboration, J. Breitweg et al., Z. Phys. **C75** (1997) 421.

[14] H1 Collaboration, T. Ahmed et al., Phys. Lett. **B348** (1995) 681.

[15] ZEUS Collaboration, M. Derrick et al., Z. Phys. **C68** (1995) 569.

[16] H1 Collaboration, C. Adloff et al., Z. Phys. **C76** (1997) 613.

[17] V. Gribov, L. Lipatov, Sov. J. Nucl. Phys. **15** (1972) 438 & 675.
Yu. Dokshitzer, JETP **46** (1977) 641.
G. Altarelli, G. Parisi, Nucl. Phys. **B126** (1977) 298.

[18] J. Bjorken, J. Kogut, Phys. Rev. **D8** (1973) 1341.
G. Bertsch, S. Brodsky, A. Goldhaber, J. Gunion, Phys. Rev. Lett. **47** (1981) 297.

[19] A. Mueller, Nucl. Phys. **B335** (1990) 115.
M. Diehl, Z. Phys. **C66** (1995) 181.

[20] M. Ryskin, Sov. J. Nucl. Phys. **52** (1990) 529.
N. Nikolaev, B. Zakharov, Z. Phys. **C53** (1992) 331.
M. Wüsthoff, Phys. Rev. **D56** (1997) 4311.

[21] J. Bartels, H. Lotter, M. Wüsthoff, Phys. Lett. **B379** (1996) 239.
J. Bartels, C. Ewerz, H. Lotter, M. Wüsthoff, Phys. Lett. **B386** (1996) 389.

[22] F. Low, Phys. Rev. **D12** (1975) 163.
S. Nussinov, Phys. Rev. Lett. **34** (1975) 1286.

[23] W. Buchmüller, A. Hebecker, Nucl. Phys. **B476** (1996) 203.

[24] W. Buchmüller, M. McDermott, A. Hebecker, Nucl. Phys. **B487** (1997) 283.
W. Buchmüller, M. McDermott, A. Hebecker, Phys. Lett. **B410** (1997) 304.

[25] J. Bartels, J. Ellis, H. Kowalski, M. Wüsthoff, DESY 98-034.

[26] H1 Collaboration, C. Adloff et al., Eur. Phys. J. **C1** (1998) 495.

[27] H1 Collaboration, C. Adloff et al., DESY 98-029, to appear in Phys. Lett. B.

[28] H1 Collaboration, C. Adloff et al., DESY 98-044, to appear in Eur. Phys. J.

[29] J. Bjorken, Phys. Rev. **D47** (1993) 101.
E. Gotsman, E. Levin, U. Maor, Phys. Lett. **B309** (1993) 199.

[30] E. Gotsman, E. Levin, U. Maor, TAUP 2485-98, hep-ph/9804404.

[31] J. Collins, L. Frankfurt, M. Strikman, Phys. Lett. **B307** (1993) 161.
A. Berera, D. Soper, Phys. Rev. **D50** (1994) 4328.
A. Berera, D. E. Soper, Phys. Rev. **D53** (1996) 6162.

[32] A. Edin, G. Ingelman, J. Rathsman, Phys. Lett. **B366** (1996) 371.

[33] P. Bruni, G. Ingelman, Proc. of the Europhysics Conference, Marseilles, France, July 1993, 595.
See also http://www3.tsl.uu.se/thep/pompyt.

[34] T. Sjöstrand, Comp. Phys. Comm. **82** (1994) 74.

[35] H. Jung, Comp. Phys. Comm. **86** (1995) 147.
See also http://www-h1.desy.de/ jung/rapgap.html.

[36] C. Weizsäcker, Z. Phys. **88** (1934) 612.
E. Williams, Phys. Rev. **45** (1934) 729.
S. Frixione, M. Mangano, P. Nason, G. Ridolfi, Phys. Lett. **B319** (1993) 339.

[37] M. Glück, E. Reya, A. Vogt, Z.Phys. **C67** (1995) 433.

[38] J. Owens, Phys. Rev. **D30** (1984) 943.

[39] M. Bengtsson, T. Sjöstrand, Z. Phys. **C37** (1988) 465.

[40] L. Lönnblad, Comp. Phys. Comm. **71** (1992) 15.

[41] T. Sjöstrand, Comp. Phys. Comm. **39** (1986) 347.
T. Sjöstrand, M. Bengtsson, Comp. Phys. Comm. **43** (1987) 367.

[42] J. Theissen, PhD Thesis (Aachen University), 1997 (in German).

[43] B. Laforge, PhD Thesis (Paris XI - Orsay University), 1997 (in French).

[44] H1 Collaboration, I. Abt et al., Nucl. Instr. and Meth. **A386** (1997) 310 & 348.

[45] J. Huth et al., Proc. of the 1990 DPF Summer Study on High Energy Physics, Snowmass, ed. E. Berger, World Scientific (1992) 134.

[46] H1 Collaboration, T. Ahmed et al., Nucl. Phys. **B445** (1995) 195.

[47] G. Schuler, H. Spiesberger, Proc. of the Workshop Physics at HERA, Vol. 3, eds. W. Buchmüller, G.Ingelman, DESY (1992) 1419.

[48] R. Engel, Z. Phys. **C66** (1995) 203.
R. Engel, J. Ranft, Phys. Rev. **D54** (1996) 4244.

[49] B. List, `Diffraktive J/ψ–Produktion in Elektron–Proton–Stößen am Speicherring HERA', Diploma Thesis (Tech. Univ. Berlin), 1993 (unpublished).

[50] S. Baranov, O. Dünger, H. Shooshtari, J. Vermaseren, Proc. of the Workshop Physics at HERA, Vol. 3, eds. W. Buchmüller, G.Ingelman, DESY (1992) 1478.

[51] H1 Collaboration, S. Aid et al., Z. Phys. **C69** (1995) 27.

[52] H. Spiesberger, H. Möhring, Comp. Phys. Comm. **69** (1992) 155.

[53] H. Abramowicz, K. Charchuła, A. Levy, Phys. Lett. **B269** (1991) 458.

[54] H1 Collaboration, C. Adloff et al., Eur.Phys.J. **C1** (1998) 97.

[55] ZEUS Collaboration, J. Breitweg et al., Phys. Lett. **B421** (1998) 368.

[56] H1 Collaboration, S. Aid et al., Z. Phys **C70** (1996) 17.

[57] F. Bopp, R. Engel, J. Ranft, A. Rostovtsev, Proc. of PHOTON'97, Egmond aan Zee, The Netherlands, eds. A. Buijs, F. Erné, World Scientific (1998) 353.

[58] L. Alvero, J. Collins, J. Terron, J. Whitmore, CTEQ-701, hep-ph/9805268.

[59] ZEUS Collaboration, M. Derrick et al., Phys. Lett. **B369** (1996) 55.
H1 Collaboration, 'Rapidity Gaps between Jets in Photoproduction at HERA', paper 380 submitted to the Int. Europhysics Conf. on H.E.P, Jerusalem, Israel, August 1997.
D0 Collaboration, S. Abachi et al., Phys. Rev. Lett. **76** (1996) 734.
CDF Collaboration, F. Abe et al., Phys. Rev. Lett. **80** (1998) 1156.

[60] A. Donnachie, P. Landshoff, Nucl. Phys. **B244** (1984) 322.
A. Donnachie, P. Landshoff, Nucl. Phys. **B303** (1988) 634.

[61] A. Hebecker, Nucl. Phys. **B505** (1997) 349.

[62] G. Ingelman, A. Edin, J. Rathsman, Comp. Phys. Commun. **101** (1997) 108.

(a)

$p_T^{\rm jet}$ (GeV)	$\mathrm{d}\sigma/\mathrm{d}p_T^{\rm jet}$ (pb GeV^{-1})	Stat. error (pb GeV^{-1})	Syst. error (pb GeV^{-1})	
			Uncorrelated	Correlated
5 - 7	462.	25.	52.	103.
7 - 9	153.	13.	21.	34.
9 - 11	49.7	6.7	7.4	11.1
11 - 13	6.65	2.30	2.17	1.49

(b)

$p_T^{\rm jet}$ (GeV)	$\mathrm{d}\sigma/\mathrm{d}p_T^{\rm jet}$ (pb GeV^{-1})	Stat. error (pb GeV^{-1})	Syst. error (pb GeV^{-1})	
			Uncorrelated	Correlated
5 - 7	43.3	6.2	9.4	3.4
7 - 10	8.82	1.78	1.65	0.71

(c)

$\eta_{\rm lab}^{\rm jet}$	$\mathrm{d}\sigma/\mathrm{d}\eta_{\rm lab}^{\rm jet}$ (pb)	Stat. error (pb)	Syst. error (pb)	
			Uncorrelated	Correlated
-1.0 - -0.5	628.	61.	64.	140.
-0.5 - 0.0	717.	60.	83.	160.
0.0 - 0.5	623.	56.	72.	139.
0.5 - 1.0	398.	41.	49.	89.
1.0 - 1.5	197.	29.	21.	44.
1.5 - 2.0	115.	26.	11.	26.

(d)

$x_\gamma^{\rm jets}$	$\mathrm{d}\sigma/\mathrm{d}x_\gamma^{\rm jets}$ (pb)	Stat. error (pb)	Syst. error (pb)	
			Uncorrelated	Correlated
0.2 - 0.4	469.	71.	57.	85.
0.4 - 0.6	762.	93.	106.	137.
0.6 - 0.8	1180.	120.	150.	210.
0.8 - 1.0	806.	98.	89.	145.

(e)

$z_{I\!P}^{\rm jets}$	$\mathrm{d}\sigma/\mathrm{d}z_{I\!P}^{\rm jets}$ (pb)	Stat. error (pb)	Syst. error (pb)	
			Uncorrelated	Correlated
0.2 - 0.4	1130.	140.	170.	200.
0.4 - 0.6	938.	99.	112.	169.
0.6 - 0.8	732.	85.	70.	132.
0.8 - 1.0	242.	52.	23.	44.

(f)

$z_{I\!P}^{\rm jets}$	$\mathrm{d}\sigma/\mathrm{d}z_{I\!P}^{\rm jets}$ (pb)	Stat. error (pb)	Syst. error (pb)	
			Uncorrelated	Correlated
0.2 - 0.4	117.	32.	25.	9.
0.4 - 0.6	67.7	21.7	11.8	5.4
0.6 - 0.8	20.2	10.2	5.1	1.6
0.8 - 1.0	7.09	6.31	2.33	0.57

Table 2: Tables summarising the data points shown in figures 4 – 6 for the kinematic regions specified in table 1. Differential cross sections, statistical errors, systematic errors that vary from data point to data point and overall normalisation uncertainties are given. (a,b) The photoproduction (a) and DIS (b) cross sections differential in the jet momentum transverse to the $\gamma^{(*)}I\!P$ interaction axis in the rest frame of X. (c) The photoproduction cross section differential in laboratory pseudorapidity. (d) The photoproduction cross section differential in $x_\gamma^{\rm jets}$. (e,f) The photoproduction (e) and DIS (f) cross sections differential in $z_{I\!P}^{\rm jets}$. There is one entry in the cross section per jet in (a – c) and one entry per event in (d – f).